
Figures and figure supplements

Adult-born granule cells mature through two functionally distinct states

János Brunner, et al.

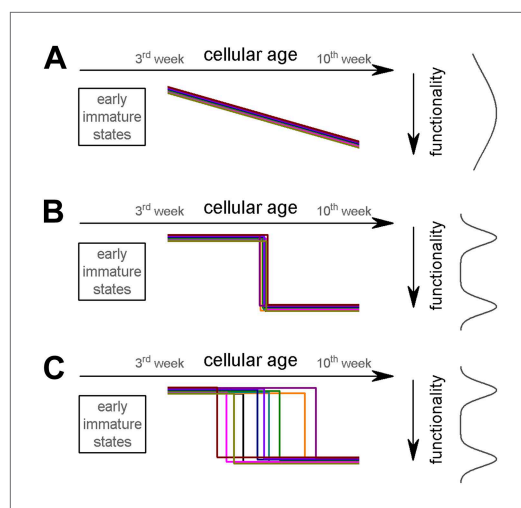


Figure 1. Potential theoretical modes of postmitotic maturation of functional properties. Each colored line represents the age-dependent change of a theoretical parameter from individual ABGCs. **(A)** Gradual maturation of the properties results in widely distributed functional continuum. **(B)** Temporally predefined functional switch. **(C)** The functional switch occurs in an extended temporal window.

DOI: [10.7554/eLife.03104.003](https://doi.org/10.7554/eLife.03104.003)

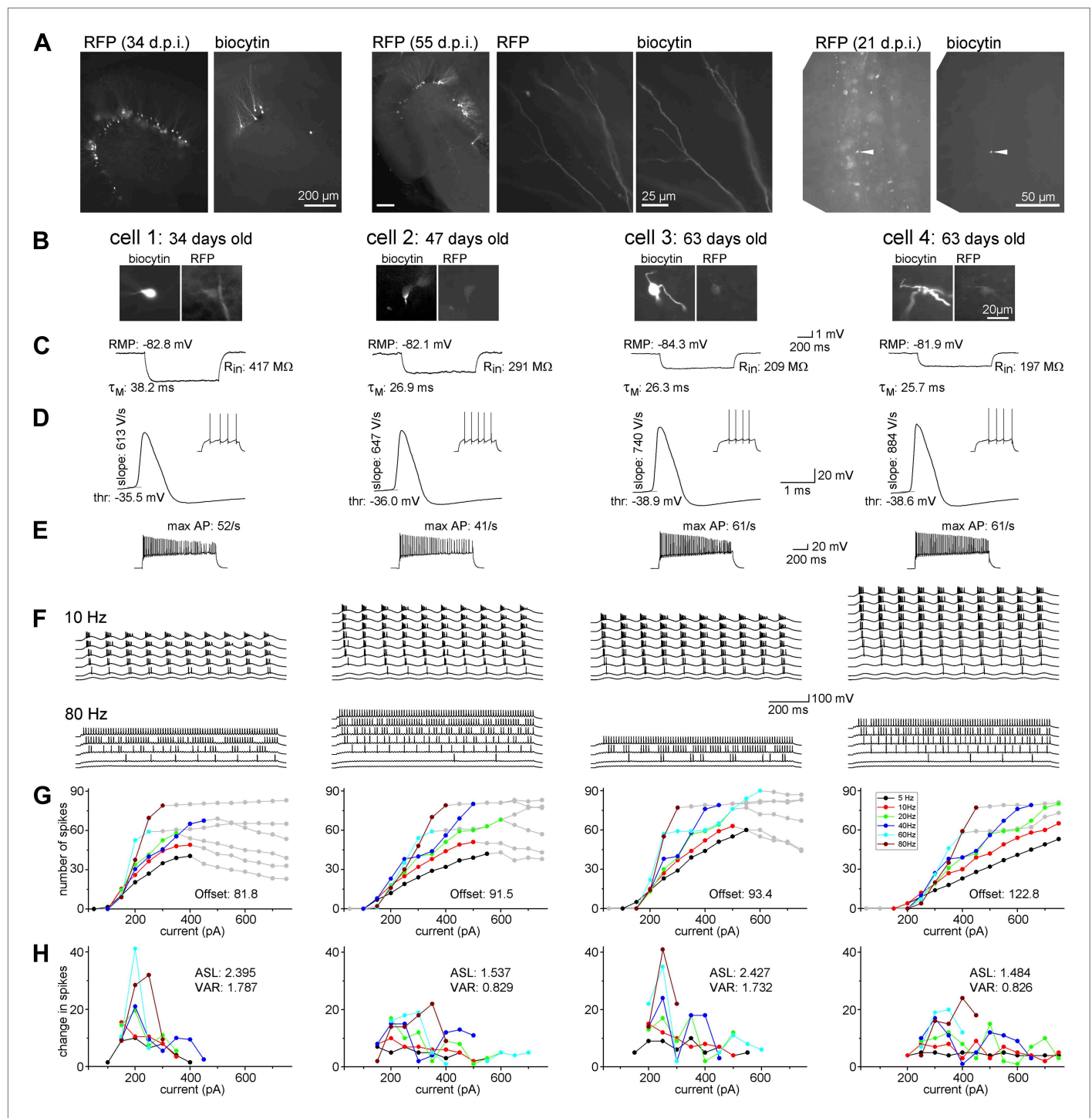


Figure 2. Maturation of the biophysical and integrative properties of ABGCs. **(A)** The RFP and biocytin-labeled cells in the dentate gyrus (left panels, d.p.i.: day after virus injection), spiny dendrites (middle panels), and typical mossy fiber terminals in the stratum lucidum of the CA3 region (right) confirm granule cell identity. **(B)** Four representative RFP-expressing granule cells 34, 47, and 63 days after CAG-RFP virus labeling. The 63-day-old ABGCs were recorded from the same slice. **(C)** Average subthreshold voltage responses of the example cells to small (~ 10 pA) current steps. Input resistance (R_{in}), membrane time constant (τ_M), and resting membrane potential (RMP) of the cells are indicated. **(D)** Spike parameters of the example cells at lower current intensities (dV/dt : maximal rate of rise, thr: action potential threshold). **(E)** Maximal firing rate of the four cells in response to square pulse current injection. **(F)** Responses of the cells to sinusoidal current injections with increasing amplitude ($\Delta 50$ pA) at 10 and 80 Hz. The traces are shown until the firing reached saturation. **(G)** Number of spikes generated in the example cells as a function of the peak amplitude of the injected sinusoid currents at the all tested frequencies. Gray symbols indicate values that were omitted from the analysis due to lack or saturation of spiking. Offset values describe Figure 2. *Continued on next page*

Figure 2. Continued

the minimum input intensities to reach 50% spiking output. **(H)** Increments of the firing (i.e., the first derivative of the curves in panel **F**) of the cells. These values were used for the calculation of the average slope (as mean, ASL) and the variance of firing (as variance, VAR). Note that cells 1 and 3 have exceptionally large values at certain input intensity ranges indicating that these cells were more sensitive to certain input intensities. This characteristic is quantified by the large VAR value.

DOI: [10.7554/eLife.03104.004](https://doi.org/10.7554/eLife.03104.004)

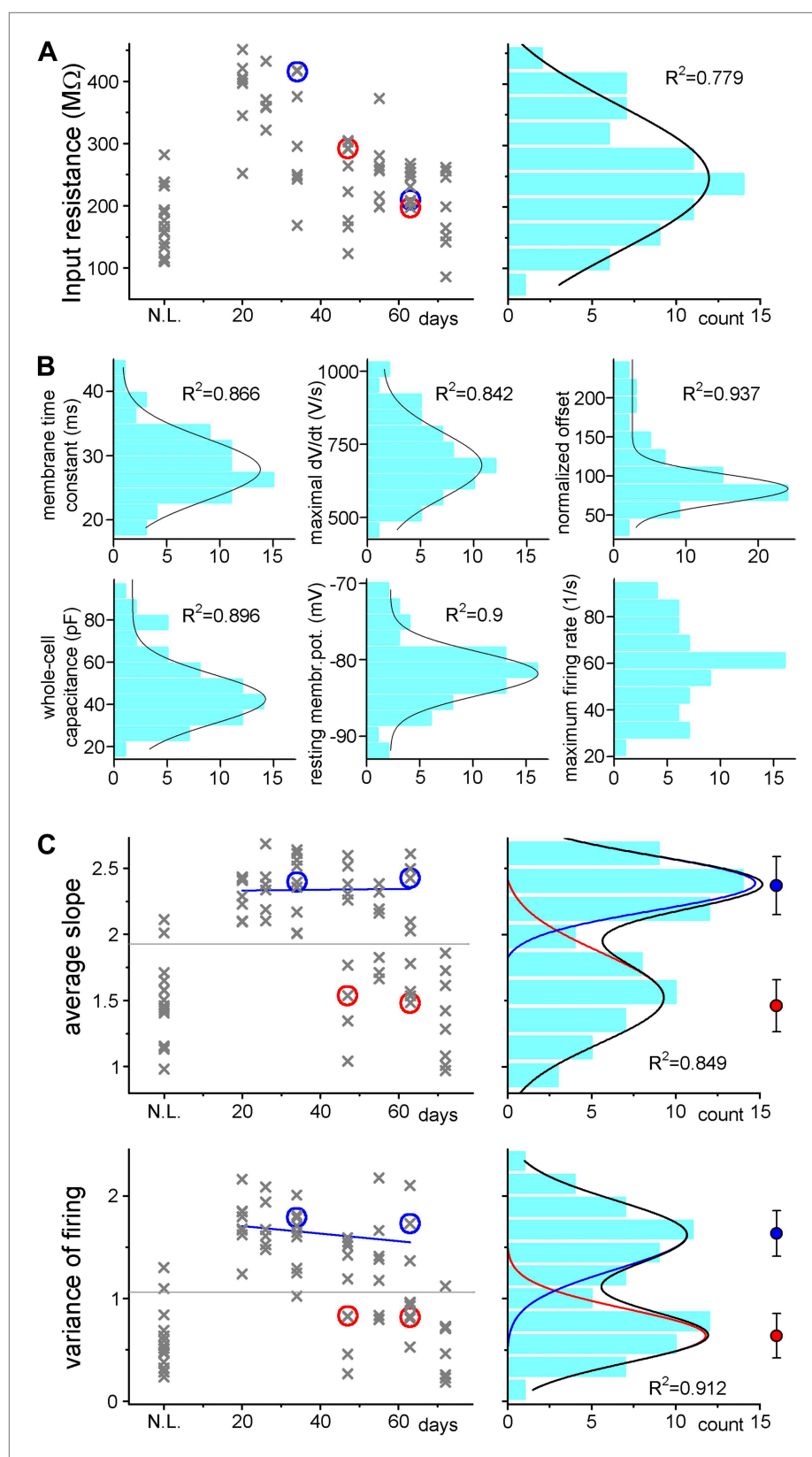


Figure 3. Adult born granule cells (3–10 week old) can be divided into two distinct populations based on cell-to-cell differences in input–output transformation. **(A)** Left, input resistance of individual ABGCs with various ages (gray crosses). Red and blue circles (S- and L-group members, respectively) highlight the values for the example Figure 3. Continued on next page

Figure 3. Continued

cells shown in **Figure 1**. N.L.: not labeled control cells. Right, probability distribution of the data set shows single peak (single Gaussian fit: $F = 0.0001$). **(B)** Monotonous probability distribution of membrane time constant, whole cell capacitance, resting membrane potential, maximal rate of rise of spikes, relative offset of the input–output curves, and action potential threshold data from the same set of cells as above. **(C)** Left, average slope (top) and variance of the slope (bottom) of the same individual ABGCs as above with various ages (gray crosses). Blue lines indicate the lack of correlation between the gain of the input–output functions and the age of individual cells within the S-group (linear fit, ASL: $R^2 = -0.029$, $p = 0.89$, VAR: $R^2 = 0.01$, $p = 0.257$). Right, two population emerges from the distribution of the average slope values of individual cells (two peaks Gaussian, ASL: $F = 0.0014$, VAR: $F = 0.0001$). The centers of the two clusters and average distance values from the centers (error bars) are shown on the right (K-means analysis, $F < 10^{-9}$, horizontal gray lines on the left panels indicate the separation by the K-means analysis).

DOI: [10.7554/eLife.03104.005](https://doi.org/10.7554/eLife.03104.005)

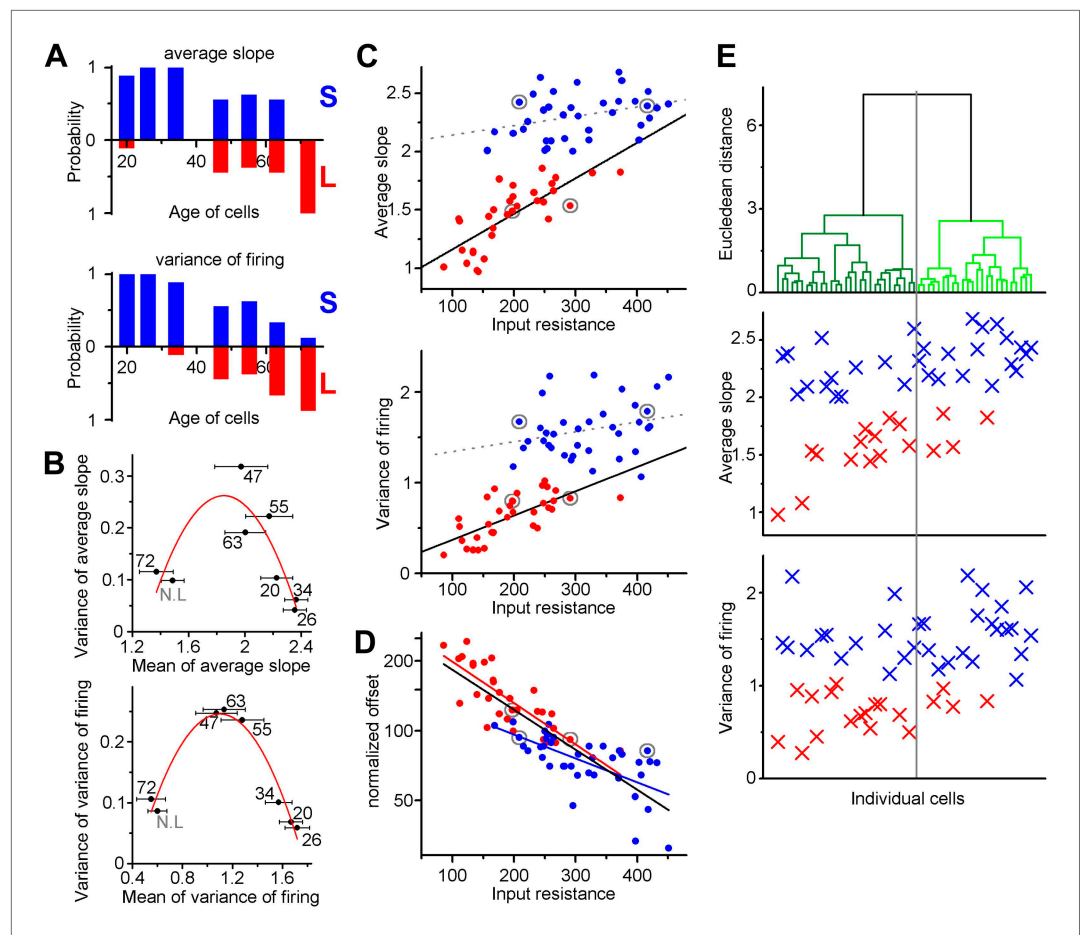


Figure 4. Independence of the output properties of individual ABGCs from age and input resistance. **(A)** Probability of the members of the clusters defined by the K-means analysis continuously shifts from S-group (blue) toward L-group (red) during maturation indicating the higher prevalence of ABGCs with shallow and invariable input–output function. **(B)** The population level functional switch is also suggested by the higher variance of the input–output parameters during the transition age period and low variance in the youngest and most matured populations (parabolic fit, ASL: $R^2 = 0.611$, $F(\text{ANOVA}) = 0.0035$; VAR: $R^2 = 0.853$, $F = 0.00017$). Numbers indicate the age of the data sets. **(C)** Correlation of the integrative parameters to the input resistance within the two functionally different groups (red and blue symbols) defined by K-means cluster analysis (see **Figure 3**). Gray circles indicate the four example cells from **Figure 2** (linear fits, ASL: $R^2 = 0.087$, $p = 0.045$ for S-group, $R^2 = 0.576$, $p = 2.9 \times 10^{-7}$ for L-group; VAR: $R^2 = 0.02$, $p = 0.19$ for S-group $R^2 = 0.467$, $p = 2.6 \times 10^{-6}$ for L-group). **(D)** Correlation between the normalized current needed to reach output that is half of the input frequency and input resistance of individual ABGCs belonging to the two functionally different groups ($R^2 = 0.39$, $p = 0.0001$ for S-group; $R^2 = 0.607$, $p = 2 \times 10^{-8}$ for L-group; $R^2 = 0.682$, $p < 10^{-8}$ for both groups). **(E)** Considering multiple membrane parameters of the individual cells (resting membrane potential, membrane time constant, whole cell capacitance, input resistance, threshold, peak dV/dt , maximal firing rate) for hierarchical cluster analysis (Ward method with normalized values) were not sufficient to predict the functional identity of the cells. Data from individual cells are aligned vertically (lines in the upper panel and symbols in the middle and bottom panels). Thus, the order of the points along the X-axes is determined by the results of the cluster analysis.

DOI: [10.7554/eLife.03104.006](https://doi.org/10.7554/eLife.03104.006)

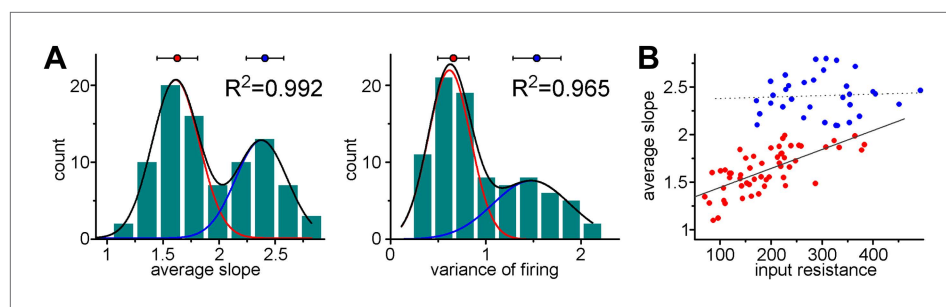


Figure 4—figure supplement 1. Coexistence of S- and L-functionalities among granule cells from non-labeled animals.

DOI: [10.7554/eLife.03104.007](https://doi.org/10.7554/eLife.03104.007)

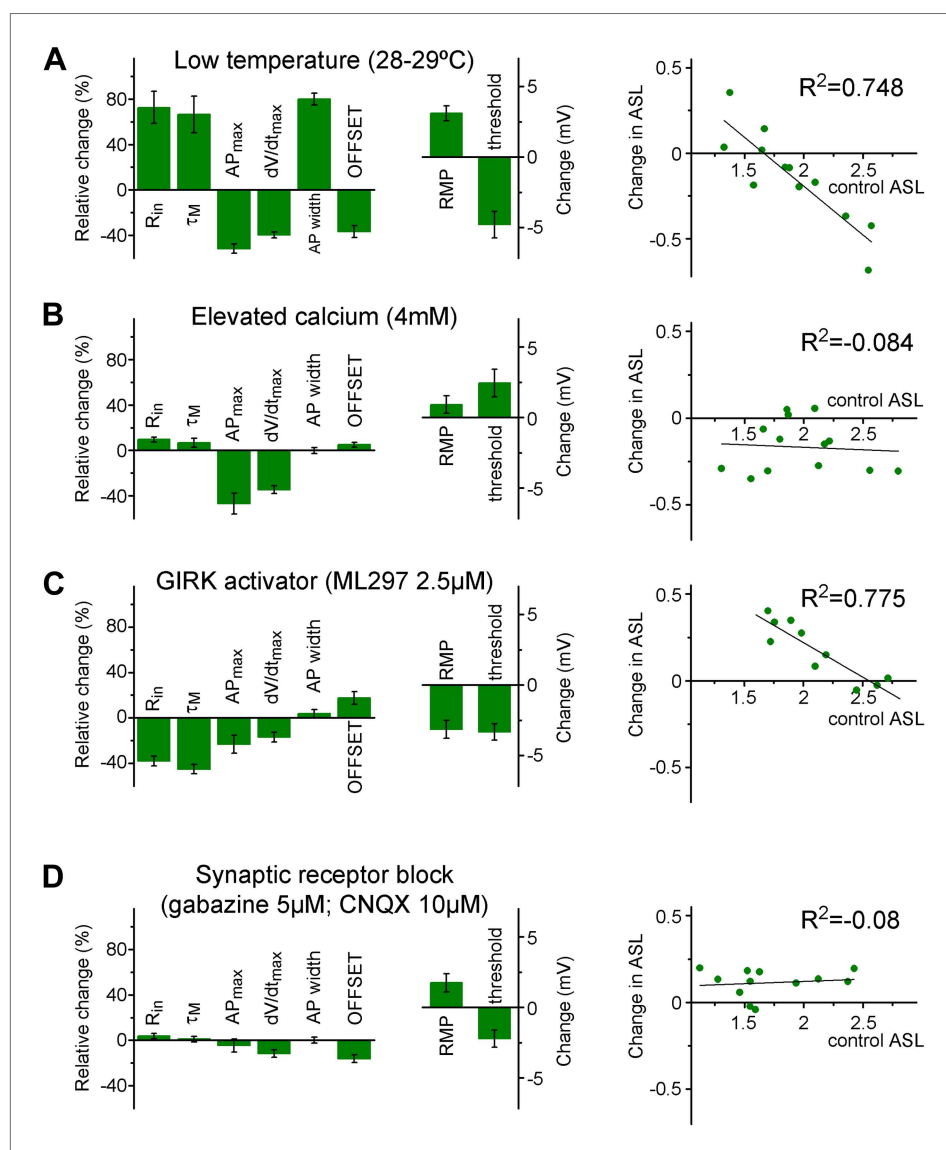


Figure 4—figure supplement 2. The input-output transformation of individual cells is maintained in two stable states by complex mechanisms.

DOI: [10.7554/eLife.03104.008](https://doi.org/10.7554/eLife.03104.008)